ELSEVIER

Journal of Organometallic Chemistry 637–639 (2001) 710–718

Journal of Organometallic Chemistry

www.elsevier.com/locate/jorganchem

Synthesis and characterisation of rhodium(0) and rhodium(−1) complexes stabilised by 1,1′-bis(diphenylphosphino)ferrocene (dppf). Crystal structures of $[Rh(dppf)_2]$ and $[Na(THF)_5][Rh(dppf)_2]\cdot THF$

Bruno Longato [a,b,*], Roberto Coppo [b], Giuseppe Pilloni [b], Carlo Corvaja [c], Antonio Toffoletti [c], Giuliano Bandoli [d]

[a] *Centro di Studio sulla Stabilita' e Reattivita' dei Composti di Coordinazione, C.N.R., Via Marzolo 1, 35131 Padua, Italy*
[b] *Dipartimento di Chimica Inorganica, Metallorganica ed Analitica, Universita' di Padova, Via Marzolo 1, 35131 Padua, Italy*
[c] *Dipartimento di Chimica Fisica, Universita' di Padova, Via Loredan 2, 35131 Padua, Italy*
[d] *Dipartimento di Scienze Farmaceutiche, Universita' di Padova, Via Marzolo 5, 35131 Padua, Italy*

Received 24 April 2001; received in revised form 18 May 2001; accepted 18 May 2001

Abstract

The rhodium(I) complex stabilised by the organometallic ligand 1,1′-bis(diphenylphosphino)ferrocene (dppf), $[Rh(dppf)_2]^+$ (**1**) can be electrochemically reduced to the Rh(0) and Rh(−1) species, $[Rh(dppf)_2]$ (**2**) and $[Rh(dppf)_2]^-$ (**3**), respectively, in two reversible single-electron processes. These low-valent complexes have been obtained by the chemical reduction of **1** with sodium naphtalenide in tetrahydrofuran solution and their crystal and molecular structures determined by single-crystal X-ray analyses. The anionic complex $[Rh(dppf)_2]^-$ crystallises as sodium-solvated salt, $[Na(THF)_5][Rh(dppf)_2]\cdot THF$ (**3**) in the monoclinic system. The coordination geometry around the metal in the d^{10} configuration is a slightly distorted tetrahedral in which the bite angles of the chelated diphosphines is 103° (average) and the Rh–P bond distances is in the range of 2.230(5)–2.251(5) Å. The sodium cation is surrounded by five molecules of THF in a slightly distorted trigonal-bipyramidal environment. Complex **2** is conveniently prepared by reacting equimolar amount of **1** and **3** in THF and crystallises in the triclinic system. The dihedral angle defined by the planes containing the atoms P(1)–Rh–P(2) and P(3)–Rh–P(4) is 75.2°, indicating a geometry of the rhodium in the d^9 configuration intermediately between the highly distorted square-planar (dihedral angle 49.7°), found earlier in the cationic d^8 species **1**, and in the anionic d^{10} complex (dihedral angle 95.0°). Reduction of the metal centre causes a decrease in the Rh–P bond length of 0.034 Å (average) from Rh(I) to Rh(0) and 0.071 Å from Rh(0) to Rh(−1), respectively, with a concomitant increase of the bite angle of the diphosphine which ranges from 93.4° (average) in $[Rh(dppf)_2]^+$ to 102.6° in $[Rh(dppf)_2]^-$. The EPR spectroscopic properties of **2** and the analogue iridium derivative, $[Ir(dppf)_2]$, have been examined at 20 K in 2-methyltetrahydrofuran matrix. A linear dependence between the hyperfine constants and the M–P (M = Rh, Ir) bond distances has been evidenced. This fact suggests the possibility to use the phosphorus coupling as an indication of the metal–phosphorus bond length in similar complexes.

Keywords: Rhodium complexes; Ferrocenyl phosphine; Zero-valent complexes; Crystal structures; Rhodium and iridium ESR

1. Introduction

Complexes of rhodium in low oxidation states are relatively rare [1] and generally contain strong π-acidic ligands such as CO [2], PF_3 [3], bpy [4], COD [5], phosphites [6] or chelating phosphines [7]. Most of them have the metal in the zero-valent state and their structures have been inferred by electron paramagnetic resonance spectroscopic studies [8]. Only recently the first examples of Rh(0) and Rh(−1) complexes structurally characterised by single crystal X-ray analysis have been described [9]. They have the metal centre

* Corresponding author. Tel.: +39-049-827-5197; fax: +39-049-827-5161.
E-mail address: longato@chin.unipd.it (B. Longato).

0022-328X/01/$ - see front matter
PII: S0022-328X(01)00984-6

stabilised by two molecules of the mixed ligand 5*H*-dibenzo[*a*,*d*]cycloepthene-5-yl]diphenylphosphine.

Earlier attempts to isolate rhodium d^9 and d^{10} species containing diphosphines such as 1,2-bis(diphenylphosphine)ethane (dppe) were prevented by the common tendency of the anionic complexes $[Rh(diphosphine)_2]^-$ to abstract a proton from the medium to give the hydride $[HRh(diphosphine)_2]$ [7].

We have recently demonstrated that the organometallic ligand 1,1′-bis(diphenylphosphino)ferrocene) (dppf), is able to stabilise the iridium atom in the oxidation states 0 and −I and the characterisation of $[Ir(dppf)_2]^0$ and $[Ir(dppf)_2]^-$ has been described [10]. The X-ray structure analysis of these redox-related complexes provided the opportunity to study the structural changes of the $\{IrP_4\}^n$ moiety on changing the charge of the complex ($n = +1, 0, -1$).

In this paper we report the synthesis and characterisation of the Rh(0) and Rh(−1) analogues, $[Rh(dppf)_2]$ (**2**) and Rh(−1) $[Rh(dppf)_2]^-$ (**3**), respectively, obtained by the stepwise reduction of the Rh(I) precursor $[Rh(dppf)_2]^+$ (**1**) [11]. The molecular structures of both these compounds have been obtained by single-crystal X-ray analyses. Moreover, a detailed study by electron paramagnetic resonance spectroscopy of the d^9 complexes $[Rh(dppf)_2]$ and $[Ir(dppf)_2]$ has been carried out in 2-methyltetrahydrofuran at 20 K. For the first time a linear dependence of the metal–phosphorus bond distances and the coupling constant of the unpaired electron with the phosphorus nuclei has been evidenced.

2. Experimental

2.1. General procedures and materials

All reactions and manipulations of solutions were carried out under a dinitrogen atmosphere of a Braun MB150 dry-box. Anhydrous tetrahydrofuran (THF), 2-methyltetrahydrofuran, toluene and hexane, purchased from Aldrich, were further purified by distillation over Na–benzophenone. 1,1′-Bis(diphenylphosphino)ferrocene, dppf, was purchased from Aldrich and used as received. Electrochemical grade tetrabutylammonium perchlorate, TBAP, was obtained from Fluka and used without further purification after drying in vacuum at 60 °C. High purity argon, further purified from oxygen by passing over reduced copper at 450 °C, was used in the electrochemical experiments. $[Rh(dppf)_2]X$ ($X = BPh_4$, **1a**) was prepared as previously reported [11].

2.2. Apparatus

^1H- and $^{31}P\{^1H\}$-NMR spectra were obtained at 298 K in 5 mm sample tubes on a Bruker 400 AMX and/or on a JEOL 90 MHz spectrometer. The external reference was H_3PO_4 (85% w/w in H_2O) for ^{31}P spectra. ^1H chemical shifts are referred to the residual peak(s) of the deuterated solvents used (Aldrich). IR and electronic spectra were obtained using a Nicolet 5SXC-FTIR and a Cary 5E spectrometer, respectively. ESR spectra were recorded with a Bruker ER 200 D X-band spectrometer, equipped with a helium flow cryostat (Oxford ESR 900). The samples were sealed under vacuum in quartz tubes after repeated freeze–pump–thaw cycles to avoid any oxygen contamination.

All electrochemical experiments were carried out in anhydrous deoxygenated THF solutions with 0.2 mol dm^{-3} TBAP as the supporting electrolyte, using a conventional three-electrode liquid-jacketed cell. Cyclic voltammetry (CV) measurements were carried out with an Amel 551 potentiostat modulated by an Amel 566 function generator. The recording device was an Amel model 863 *X*–*Y* recorder. The working electrode was a planar gold microelectrode freshly coated with mercury (ca. 0.4 mm^2) surrounded by a platinum spiral counter electrode. Controlled potential electrolyses were carried out with an Amel 552 potentiostat linked to an Amel 731 digital integrator. The working electrode was a mercury pool (ca.12 cm^2), and the counter electrode was external, the connection being made through an appropriate salt bridge. In all cases silver/0.1 mol dm^{-3} silver perchlorate in acetonitrile, separated from the test solution by 0.2 mol dm^{-3} TBAP in THF solution sandwiched between two fritted disks, was used as the reference electrode. Compensation for *iR* drop was achieved by a positive feedback. Ferrocene was added at the end of each experiment as the internal reference. All potentials are referred to the ferrocenium/ferrocene redox couple ($E_{1/2} = +0.080$ V relative to the actual $Ag/AgClO_4$ reference electrode and +0.535 V vs. aq. SCE under the present experimental conditions).

2.3. Preparation of the complexes

2.3.1. $[Rh(dppf)_2]BF_4$ (*1b*)

A solution of $AgBF_4$ (395 mg, 2.03 mmol) in acetone (30 ml) was added to a solution of $[RhCl(C_8H_{12})]_2$ [12] (500 mg, 1.01 mmol) in acetone (30 ml) at room temperature (r.t.) under nitrogen. The precipitate of AgCl formed immediately was filtered after a few minutes and the filtrate was added to a solution of dppf (2.24 g, 4.05 mmol) in CH_2Cl_2 (40 ml). Heating the resulting solution at reflux temperature for 1.5 h determined the formation of a yellow precipitate. The mixture was evaporated under vacuum and the orange residue dissolved in a minimum amount of CH_2Cl_2. Addition of MeOH (45 ml) formed a yellow precipitate, which was collected by filtration, washed with MeOH dried under vacuum to a constant weight (2.07 g). The isolated solid contains ca. 1 mol of CH_2Cl_2 per mol of

the rhodium complex. Yield: 79%. Anal. Found: C, 59.76; H, 4.26. Calc. for $C_{69}H_{58}P_4Cl_2BF_4Fe_2Rh$: C, 59.10; H, 4.08%. ^{1}H-NMR ($CDCl_3$, δ ppm): 7.3 (br s, 40H, Ph), 5.27 (s, 2H, CH_2Cl_2), 4.11 (br s, 8H, Cp), 3.64 (br s, 8H, Cp). $^{31}P\{^1H\}$-NMR ($CDCl_3$, 36.23 MHz): δ 22.2 (d, [$^1J_{Rh-P} = 139$ Hz]).

2.3.2. [Rh(dppf)$_2$] (2)

A solution of $[Na(THF)_2][Rh(dppf)_2]$ (**3**) (109 mg, 7.98 mmol) in 4 ml of a mixture of THF–toluene (1:1 v/v) was added to a suspension of **1b** (105 mg, 8.08 mmol) in THF (3 ml). The resulting deep-red solution was stirred for 10 min and then concentrated under vacuum to a small volume (ca. 3 ml) to induce the precipitation of $NaBF_4$ and then filtered off. The addition of hexane caused the precipitation of a powdered red solid, which was collected by filtration, washed with hexane and dried under vacuum. **2**: Yield: 168 mg (86%). Anal. Found: C, 66.92; H, 4.47. Calc. for $C_{68}H_{56}P_4Fe_2Rh$: C, 67.40; H, 4.66%. Vis–NIR spectrum in THF: λ_{max} 745 nm ($\varepsilon \approx 980$ $M^{-1}\,cm^{-1}$). $^{31}P\{^1H\}$-NMR spectrum in toluene-d_8–THF (1:1 v/v): no resonances.

2.3.3. [Na(THF)$_2$][Rh(dppf)$_2$] (3)

To a suspension of **1b** (250 mg, 0.19 mmol) in THF (5 ml) were added 1.55 ml of a 0.34 mol dm^{-3} THF solution of sodium naphtalenide (three equivalents). A deep-red solution was immediately obtained which rapidly turned to a black mixture. A small amount of metallic Na was then added (a few milligrams) and the mixture was stirred at r.t. for 1 h. The reaction mixture was filtered, concentrated under vacuum at ca. 1/2 of the initial volume and the precipitate of $NaBF_4$ formed was filtered off. Addition of hexane gave an brown–black solid which was collected by filtration, washed with hexane and carefully dried under vacuum to give 210 mg of a black solid $[Na(THF)_2][Rh(dppf)_2]$ (**3**). Yield: 80%. Anal. Found: C, 66.11; H, 4.92. Calc. for $C_{76}H_{72}O_2P_4Fe_2NaRh$: C, 66.19; H, 5.26%. ^{1}H-NMR (THF-d_8, δ ppm): 7.55 (br s, 16H, Ph), 6.64 (br s, 24H, Ph), 3.91 (s, 8H, Cp), 3.77 (s, 8H, Cp), 3.58 (s, 8H, THF), 1.73 (complex m, 8H, THF). $^{31}P\{^1H\}$-NMR (in THF-d_8): δ 32.5 (d, $^1J_{Rh-P} = 208.6$ Hz). Visible spectrum in THF: λ_{max} 423 nm ($\varepsilon \approx 13000$ $M^{-1}\,cm^{-1}$).

2.4. X-ray crystallography

Suitable black crystals of the d^{10} species, analysed as $[Na(THF)_5][Rh(dppf)_2]\cdot THF$ (**3**), were obtained, after several days, from a saturated solution of $[Na(THF)_2][Rh(dppf)_2]$ in toluene upon vapour diffusion of hexane, at r.t. Crystals of **2** (black prisms) were obtained by layering hexane into a toluene–THF (9:1 v/v) solution of $[Rh(dppf)_2]$. The crystals were sealed in a Lindeman capillary and mounted on a Nicolet Siemens R3m/V four-circle automated diffractometer with Mo–K_α ($\lambda = 0.71073$ Å) equipped with a graphite monochromator in the incident beam. The intensities of the diffracted beam were measured at r.t. Unit cell dimensions were obtained from a least-squares fit of 50 reflections on the setting angle $2\theta > 21°$. Data were collected by the $\tilde{\omega}$-2θ scan technique, and the intensities of the two reflections were monitored periodically. The data were corrected for Lorentz-polarisation effects and for absorption (only for **2**). Unfortunately, the refinement of the crystal structure of **3** was not satisfactory and was severely hampered by two factors. In the first instance, the crystal batch had inherent handling difficulties and the only suitable sample for a single-crystal structure determination was substandard. In fact, the diffracting ability of the sample fell off rapidly with an increasing Bragg angle, and much of the higher angle data collected was flagged as weak and bore negative intensity. As a consequence, the data collection was restricted to $2\theta_{max} = 40°$ (while for **2** $2\theta_{max}$ was 50°). Secondly, the black parallelepiped ($0.1 \times 0.30 \times 0.05$ mm^3) was sensitive toward X-rays and decomposed after a three-day irradiation. Decay correction was applied, while no absorption correction was applied to the intensity data.

Data collection and structure solution were carried out using the program SHELXTL/PC(1994) [13] and SHELXL/93(1993) [14]. The structures were solved by the Patterson method for heavy atoms with refinement on F^2 by standard full-matrix least-squares. In the last cycles of refinement of **2** the Fe, P, O and C atoms were allowed to vibrate anisotropically, and the H atoms included in ideal positions. For **3** only the Rh, Fe, P and Na atoms were allowed to vibrate anisotropically. The phenyl and cyclopentadienyl rings were refined as rigid bodies, with C–C and C–H distances fixed at 1.395 and 1.08 Å, respectively. Anisotropy was introduced only for the non-carbon atoms and for the tetrafluoroborate anion. Crystallographic data and reliability factors are reported in Table 1.

3. Results and discussion

3.1. Electrochemistry

The electrochemical pattern of $Rh(dppf)_2]BPh_4$ in THF 0.2 M TBAP is virtually identical with that found in the reduction of the closely related iridium compound [10]. A typical voltammogram is shown in Fig. 1.

It is apparent that the complex undergoes two discrete, fully reversible, one-electron reductions centred at $E^1_{1/2} = -1.525$ Vand $E^2_{1/2} = -1.880$ V, as mean values of the potentials for negative and positive peak currents. The one noteworthy difference is a larger separa-

tion between the $E_{1/2}$ values for the two individual one-electron transfers, thus revealing a much higher stability of $[Rh(dppf)_2]^0$, compared with the iridium analogue, toward valence disproportionation. By analogy, the course of controlled-potential coulometric experiments and the redox properties of the products are those expected from the voltammetric profile of the depolariser, i.e. one electron/molecule is required for each reduction step, and the reduced species show cyclic voltammetric peaks, positive and/or negative according to the oxidation state, at the appropriate potentials. Exhaustive electrolysis at the first process leads to a dark-brown, highly air-sensitive solution which exhibits a well-resolved ligand field band at λ_{max} 745 nm ($\varepsilon \approx$ 980 $M^{-1}\,cm^{-1}$) and gives a strong ESR signal with a hyperfine structure consistent with coupling of the unpaired electron with four equivalent ^{31}P atoms. Further reduction of the dark-brown solution or exhaustive electrolysis of $[Rh(dppf)_2]^+$ at potentials past the second reduction peak produces a red–orange solution which is ESR silent and displays only a strong absorption band at $\lambda_{max} = 423$ nm ($\varepsilon \approx 13{,}000$ $M^{-1}\,cm^{-1}$) ascribable to a charge-transfer transition. The following scheme summarises the experimental results:

$$[Rh(dppf)_2]^+ \;\overset{e}{\rightleftharpoons}\; [Rh(dppf)_2]^0 \;\overset{e}{\rightleftharpoons}\; [Rh(dppf)_2]^- \quad (1)$$

whence

$$[Rh(dppf)_2]^+ + [Rh(dppf)_2]^- \rightleftharpoons 2\,[Rh(dppf)_2]^0 \quad (2)$$

$$K = \frac{[Rh(dppf)_2]^2}{\{[Rh(dppf)_2]^+[Rh(dppf)_2]^-\}} \approx 1 \times 10^6 \text{ at } 25\ ^\circ\text{C in THF}$$

On the basis of the above Eq. (1) and in view of the successful chemical procedure adopted for the redox-related pairs of iridium analogues, the Rh(−1) species has been prepared by the reduction of the cationic precursor **1b** employing sodium naphtalenide as the reducing agent, while the Rh(0) complex has been obtained according to Eq. (2) by reacting equimolar amounts of Rh(I) and Rh(−1) counterparts (see Chart 1).

Table 1
Crystallographic data for complexes $[Rh(dppf)_2]$ (**2**) and $[Na(THF)_5][Rh(dppf)_2]\cdot THF$ (**3**)

	$[Rh(dppf)_2]$	$[Na(THF)_5][Rh(dppf)_2]\cdot THF$
Empirical formula	$C_{68}H_{56}P_4Fe_2Rh$	$C_{92}H_{104}O_6P_4Fe_2NaRh$
Formula weight	1211.62	1667.23
Temperature (°C)	21	21
Wavelength (Å)	0.71073	0.71073
Space group	$P\bar{1}$ (No. 2)	$P2_1/n$ (No. 14)
Unit cell dimensions		
a (Å)	12.878(5)	13.155(8)
b (Å)	13.600(5)	23.71(1)
c (Å)	15.392(6)	26.48(2)
α (°)	93.99(3)	90
β (°)	90.42(3)	98.66(5)
γ (°)	92.11(3)	90
V (Å^3)	2687(2)	8165(8)
Z	2	4
ρ_{calc} (g cm^{-3})	1.1421	1.356
μ (Mo–K$_\alpha$) (cm^{-1})	30.6	20.4
R indices [a]	0.035	0.071
wR^2 [b]	0.088	0.165

[a] $R = \Sigma|\,|F_o|-|F_c|\,|/\Sigma|F_o|$.
[b] $wR^2 = [\Sigma w(F_o^2-F_c^2)^2/\Sigma w(F_o^2)^2]^{1/2}$.

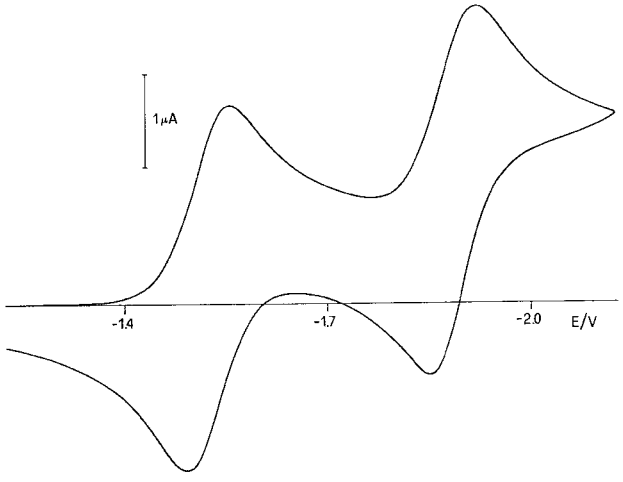

Fig. 1. Cyclic voltammogram of a 3.2 mM of $[Rh(dppf)_2]BPh_4$ (**1a**) in THF, TBAP 0.2 M, at 25 °C, scan rate 100 mV s^{-1}.

3.2. Characterisation of the Rh(−1) complex, $[Rh(dppf)_2]^-$ (3)

Addition of an excess of sodium naphthalenide (ca. three equivalents) to a THF suspension of $[Rh(dppf)_2]BF_4$ (**1b**) forms a deep-red solution which rapidly turns to maroon–black. Addition of toluene induces the precipitation of $NaBF_4$, which is easily eliminated by filtration. The Rh(−1) complex $[Rh(dppf)_2]^-$ can be isolated in quite a good yield by precipitation with hexane. The elemental analysis and the proton NMR spectrum of the solid, carefully dried under vacuum, analysed as $[Na(THF)_x][Rh(dppf)_2]$ in which x is in the 1.8–2.2 range. The ^{1}H-NMR spectrum of the black solid in THF-d_8 shows two multiplets at δ 3.58 and 1.73 attributable to THF in addition to the resonances caused by the phenyl groups (δ 7.55 and 6.64) and to the cyclopentadienyl protons (δ 3.90 and 3.77). The corresponding $^{31}P\{^1H\}$-NMR spectrum is characterised by a doublet at δ 32.5, arising from the coupling of the phosphorus atoms with the ^{103}Rh nucleus ($^1J_{P-Rh} = 209$ Hz), in agreement with the presence of chemically and magnetically equivalent dppf ligands.

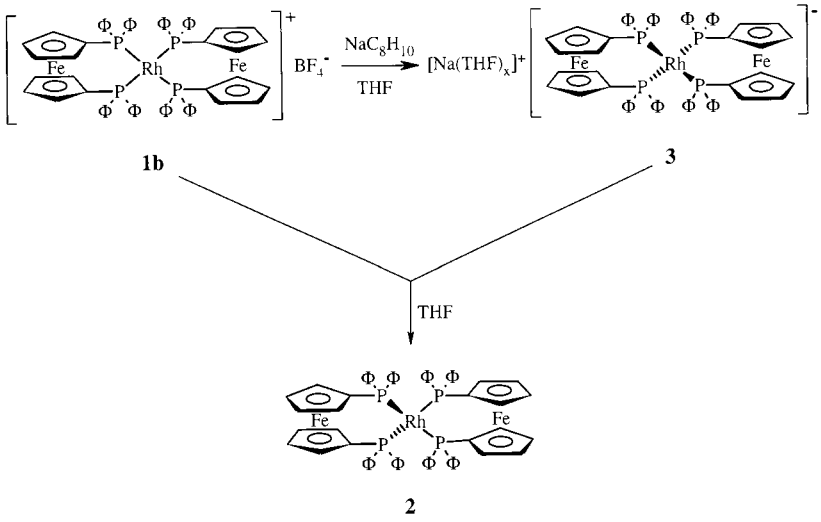

Chart 1.

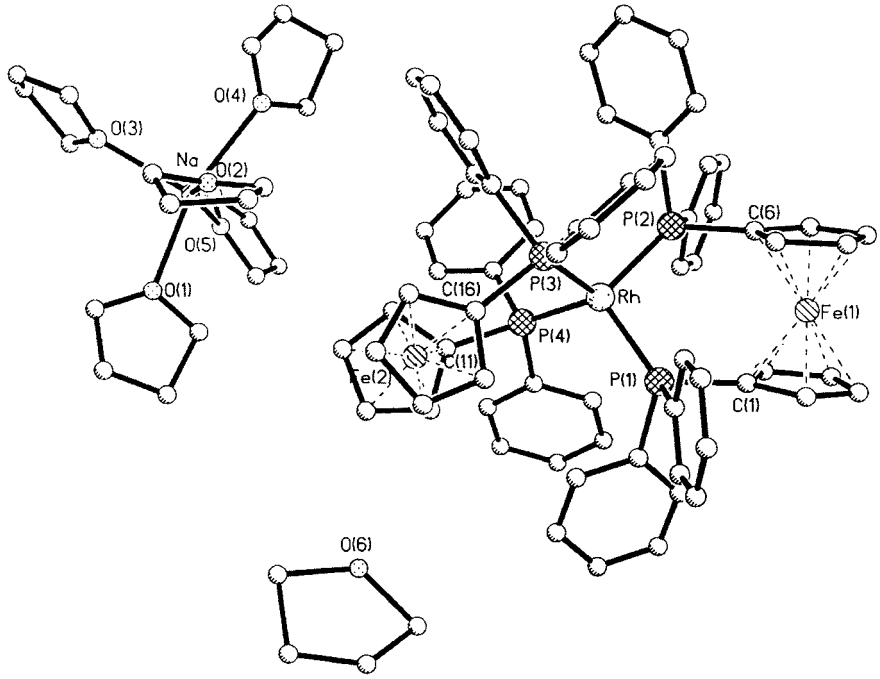

Fig. 2. Crystal structure of $[Na(THF)_5][Rh(dppf)_2]\cdot THF$ (**3**).

The crystals obtained by the vapour diffusion of hexane into a saturated solution of $[Na(THF)_2]$-$[Rh(dppf)_2]$ in toluene have the composition $[Na(THF)_5][Rh(dppf)_2]\cdot THF$ as deduced by the X-ray analysis. The structure of this sodium solvated salt (**3**) is depicted in Fig. 2 and the main bond distances and bond angles are listed in Table 2.

The anion $[Rh(dppf)_2]^-$ contains the Rh atom bound to two chelated dppf molecules in a slightly distorted tetrahedral environment. The co-ordination planes of the ligands, defined by the atoms P(1)–Rh–P(2) and P(3)–Rh–P(4), respectively, form a dihedral angle of 95.0°, but only two of the P–Rh–P angles approach the ideal value of 109.5°. Particularly, the bite angle of one of the diphosphines (P(1)–Rh–P(2) = 105.2(2)° and P(3)–Rh–P(4) = 100.2(2)°), deviates significantly from the expected geometry of an 18-electron tetraco-ordinated complex. The Rh–P bond distances are in the range of 2.230(5)–2.251(5) Å with an average value of 2.244(8) Å. The cyclopentadienyl rings are staggered (*synclinal* or *gauche*), forming angles of 38.0° (Cp_1, Cp_2) and 22.9° (Cp_3, Cp_4) and slightly tilted away from the Fe centre with dihedral angles of 3.6° (Cp_1, Cp_2) and 3.4° (Cp_3, Cp_4). The notation Cp_1, Cp_2, etc., refers

to the cyclopentadienyl group bound to phosphorus atom P(1), P(2), etc.

The sodium ion is co-ordinated to the oxygen atoms of five molecules of THF in a distorted trigonal bipyramidal geometry. The oxygen atoms in the equatorial plane have distances in the range 2.28(2)–2.30(2) Å which are slightly shorter than those in the apical positions (Na–O(1) = 2.32 Å and Na–O(4) = 2.32 Å). These values are in good agreement with those found for other pentaco-ordinated sodium complexes [10]. The sixth THF molecule does not interact significantly with the sodium cation.

Table 2
Comparison of selected bond lengths (Å) and bond angles (°) for $[Rh(dppf)_2]BPh_4$ (**1**), $[Rh(dppf)_2]$ (**2**) and $[Na(THF)_5][Rh(dppf)_2]\cdot THF$ (**3**)

	1	2	3
Bond lengths			
Rh–P(1)	2.311(3)	2.306(1)	2.230(5)
Rh–P(2)	2.407(4)	2.323(1)	2.250(5)
Rh–P(3)	2.358(3)	2.312(1)	2.244(5)
Rh–P(4)	2.321(3)	2.318(1)	2.251(5)
Rh–P(av) [a]	2.35 [4]	2.315 [6]	2.244 [8]
Bond angles			
P(1)–Rh–P(2)	94.0(1)	102.19(4)	105.2(2)
P(3)–Rh–P(4)	92.8(2)	97.56(4)	100.2(2)
P(2)–Rh–P(3)	99.3(2)	103.95(4)	109.2(2)
P(1)–Rh–P(4)	95.4(1)	106.14(4)	109.8(2)
P(1)–Rh–P(3)	142.6(1)	120.60(4)	113.2(2)
P(2)–Rh–P(4)	146.1(1)	128.27(4)	119.7(2)
Dihedral angles			
P(1)–Rh–P(2)/P(3)–Rh–P(4)	49.7	75.2	95.0

[a] The estimated deviation in square brackets is calculated as: $\sigma = [\Sigma(x_i - \bar{x}_m)^2/n]^{1/2}$ (n = number of determinations; $\bar{x}_m$ = mean value).

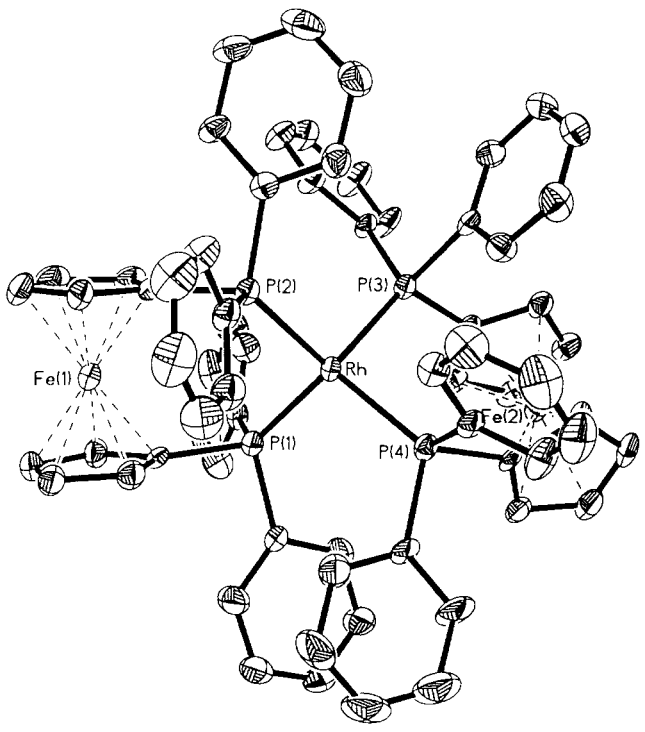

Fig. 3. Crystal structure of $[Rh(dppf)_2]$ (**2**). Thermal ellipsoids are drawn at 40% probability level.

A comparison of the structural parameters of complex **3** with those of the cationic species, $[Rh(dppf)_2]^+$ [11b], shows that when the charge of the complex changes from +1 to −1 the average of the Rh–P distances decrease by 0.10 Å and the dihedral angle formed by the co-ordination planes containing the atoms P(1)–Rh–P(2) and P(3)–Rh–P(4) increases from 49.7 to 95.0°. Very similar modifications of the metal–ligand bond distances were observed in the iridium analogues, $[Ir(dppf)_2]^n$ ($n = +1, 0, -1$) [10] and were interpreted as an increasing contribution of the $M \rightarrow P\pi$ bonding as the formal charge of the metal is decreased. The shortening of the Rh–P bonds as a result of the addition of electrons to the metal is accompanied by a twist of the four donor atoms toward a tetrahedral arrangement, the expected geometry of the ligands in a four co-ordinate complex with d^{10} configuration. However, a shorter metal–ligand distance in the anionic complexes can also be favoured by a reduced crowding of the co-ordination sphere in the tetrahedral environment.

3.3. Characterisation of the Rh(0) complex, $[Rh(dppf)_2]$ (2)

As anticipated on the basis of the cyclovoltammetric analysis, Rh(0) complex **2** can be conveniently prepared according to Eq. (2) by reacting equimolar amounts of **1b** and **3** in THF solution (Chart 1). The X-ray structure of this complex is shown in Fig. 3 and the relevant bond distances and bond angles are reported in Table 2.

The geometrical environment of the Rh atom in $[Rh(dppf)_2]$ is in between the highly distorted square-planar $[Rh(dppf)_2]^+$ [11b] and the slightly irregular tetrahedral geometry found for $[Rh(dppf)_2]^-$. The co-ordination planes defined by the atoms P(1)–Rh–P(2) and P(3)–Rh–P(4) form a dihedral angle of 75.2° which is, in fact, intermediate between the value found in the d^8 and d^{10} species. Similarly, the average Rh–P bond distance, 2.315(6) Å, appears significantly shorter when compared with that found in the oxidised species (2.35(4) Å) and longer with respect to the average value found in the most reduced species (**3**) (2.244(8) Å). The two ligands exhibit significant differences in some structural details, the most important of them are: (i) the bite angles of the diphosphines (P(1)–Rh–P(2) = 102.19(4)°, P(3)–Rh–P(4) = 97.56(4)°); (ii) the torsion angle of the Cp rings in the ferrocenyl moieties is 39.1° for Cp_1, Cp_2 and 18.5° for Cp_3, Cp_4. This torsion is

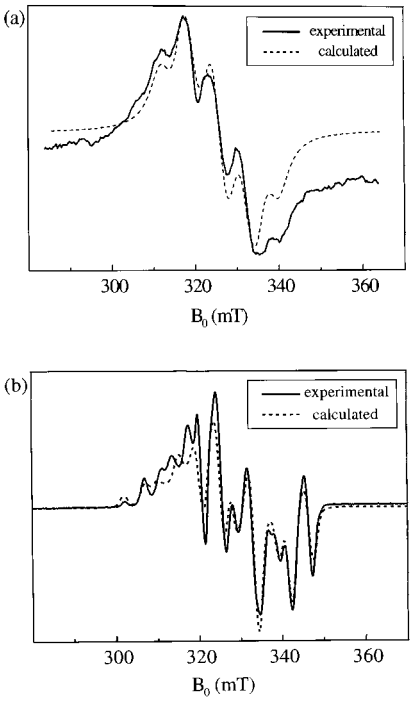

Fig. 4. ESR spectra of [Rh(dppf)$_2$] (**2**) in 2-methyltetrahydrofuran: (a) at 298 K; (b) at 20 K.

measured by the angle $C_A...X_A...X_B...C_B$ in which C_A is the carbon atom of the Cp ring 'A' bonded to the phosphorus atom, X_A the centroid of the Cp ring 'A' and C_B and X_B indicate the same positions in the Cp ring 'B'; (iii) the metal–phosphorus distances which are almost the same for one ligand (Rh–P(4) = 2.318(1) Å; Rh–P(3) = 2.312(1) Å), but exhibit the larger deviation from the average in the case of the other ((Rh–P(1) = 2.306(1) Å; Rh–P(2) = 2.323(1) Å).

A detailed ESR study of this complex, carried out in 2-methyltetrahydrofuran at 20 K, shows a clear correlation between the Rh–P bond distances and the values of the coupling constant of the unpaired electron with the phosphorus nuclei.

3.4. ESR study of [Rh(dppf)$_2$] and [Ir(dppf)$_2$]

Fig. 4 shows the EPR spectra of [Rh(dppf)$_2$] in 2-Me-THF, recorded at 298 K (a) and 20 K (b), along with the calculated spectra (dashed lines).

The first spectrum consists of a broad signal partially resolved in five hyperfine components. The second one can be roughly divided into two regions, corresponding, respectively, to the g_z value ($B_0 < 320$ mT) and to the g_x and g_y values ($B_0 > 320$ mT). The spectral lines are split into a large number of hyperfine components. The room temperature spectrum has been computer simulated by using a spin Hamiltonian including the Zeeman term and the isotropic hyperfine coupling of the $S = 1/2$ electron spin with the $I = 1/2$ ^{103}Rh nucleus and with four non-equivalent ^{31}P nuclei. It must be stressed that the simulation of the spectrum by assuming four equivalent phosphorus couplings exhibits the correct number of hyperfine components with intensity ratios 1:4:6:4:1, but does not match the experimental pattern. The coupling constants and the g value, which fit the spectrum, are reported in Table 3. They are quite similar to the values reported for [Rh(P(O-*i*-Pr)$_3$)$_4$] [8a] and for [Rh(dppe)$_2$] [8b].

In order to reproduce the 20 K spectrum, the anisotropy of the **g** tensor has been considered, while only the isotropic contributions to the hyperfine coupling have been included. The calculated spectrum shown in Fig. 4(b) shows a satisfactory agreement with the experimental one, particularly in the region corresponding to g_x and g_y. The deviation at low field, caused by neglecting the anisotropic contributions to the hyperfine constants, is not too large, indicating that the anisotropy should be small. Resulting from the presence of four different tensors with no coincident principal axes, we did not attempt a further improvement. The hyperfine couplings and **g** tensor components are reported in Table 3.

For the [Ir(dppf)$_2$] complex, the liquid solution spectrum is not informative as it consists of a single broad line [10]. Fig. 5 shows the spectrum recorded at $T = 20$ K in a frozen matrix of 2-Me–THF. It presents two wide bands overlapped partially: the low-field part, corresponding to the g_z-value, does not show any structure, while the high-field band (relative to $g_x \approx g_y$) has a partially resolved hyperfine structure. The calculated spectrum, shown in the same figure with dashed line, was obtained by including only the spin Hamiltonian isotropic hyperfine terms for the four ^{31}P nuclei as well as for the ^{191}Ir and ^{193}Ir nuclear spins, with the splitting constants reported in Table 3. The agreement between

Table 3
Hyperfine coupling constants and g values for the complexes [M(dppf)$_2$] (M = Rh, Ir)

	a_P (mT)	a_P (mT)	a_P (mT)	a_P (mT)	a_M (mT)	g_x	g_y	g_z
[Rh(dppf)$_2$] (298 K)	4.6	5.5	6.8	7.7	1.8	2.0502	2.0502	2.0502
[Rh(dppf)$_2$] (20 K)	4.80	5.50	7.50	8.50	1.00	2.0100	2.0175	2.1320
[Ir(dppf)$_2$] (20 K)	2.07	3.58	5.65	6.50	2.26	2.0100	2.0130	2.1914

Estimated error of the coupling constants is $\approx 5\%$ for $T = 298$ K and $\approx 1\%$ for $T = 20$ K.

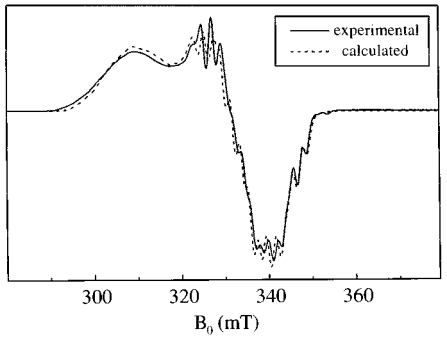

Fig. 5. ESR spectrum of $[Ir(dppf)_2]$ in 2-methyltetrahydrofuran at 20 K.

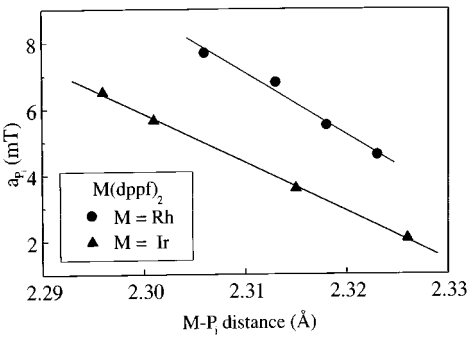

Fig. 6. Correlation between coupling constants and M–P bond lengths in $[M(dppf)_2]$.

the simulated and the experimental spectra appears to be quite good and the small differences are in line with those reported for other Ir complexes [15].

It is interesting to note that we measured four different metal to ligand distances in complex **2**, as well as in its iridium analogue. It has been suggested that the ^{31}P hyperfine coupling in metal complexes depends on the metal to ligand M–P distance. It was observed that Cr(I) complexes stabilised by phosphite ligands generally give larger couplings than those with phosphines as in the last case the M–P distance is larger [16]. In our complexes, the assignment of a particular coupling constant to a specific phosphorus nucleus is not possible. However, if we assume that the correlation between the distance and the isotropic coupling constant holds within homoleptic ligands, we can attribute the larger coupling to the nucleus at shorter distance. With this assumption, the linear dependence shown in Fig. 6 is obtained. It can be noted that the same linear dependence is obtained for both Rh and Ir complexes.

As the P_i isotropic hyperfine couplings reflect the spin density on the s orbital of phosphorus ligand atoms, we tried to correlate the s character with the M–P bond length. The value of the hyperfine coupling constant for one unpaired electron in a 3s valence orbital of a P atom has been calculated as $a_P = 365.6$ mT [17]. Using this value, the fraction of unpaired spin in the 3s orbital of the magnetically non-equivalent P_i atoms ranges from 1.3 to 2.1% for the Rh complex and from 0.6 to 1.8% for the Ir one. The origin of the 3s spin density on P atoms could arise from the spin polarisation of M–P bonds. A contribution of inner-shell s orbitals to the hyperfine coupling is not excluded [16]. The main contribution to the anisotropic coupling should come from the unpaired spin density ρ_{3p} in the 3p orbitals of the P_i atoms. For $\rho_{3p} = 1$, $A_{\parallel} = 20.7$ mT and $A_{\perp} = 10.3$ mT [17]. Even if we assume a large spin density of 5%, the calculated dipolar terms would be in the range from 0.5 to 1 mT, which confirms the small effect on the spectrum. Finally, we note that the small but significant variation of the coupling constants on changing the temperature from 298 to 20 K is in line with a decrease in the spin density on the Rh atom and an increase in spin density on the ligands.

A dependence of a_P on the Rh–P distance was suggested for explaining the line width alternation effects in the liquid solution EPR spectrum of the complex $[Rh(dppe)_2]$ (dppe = 1,2-bis(diphenylphosphino)ethane) [8b]. In that case, two different couplings were measured at low temperature (3.75 and 6.50 mT) which are of the same order of those found for **2**. Using the correlation shown in Fig. 6, the corresponding Rh–P distances in $[Rh(dppe)_2]$ would be 2.33 and 2.31 Å.

3.5. Concluding remarks

The uncommon ability of the organometallic ligand dppf in stabilising the iridium atom in low oxidation states, recently illustrated by us, has now been confirmed for the rhodium atom. Compounds **2** and **3** represent the first examples of the chelating diphosphines complexes of rhodium in the oxidation states 0 and −1 structurally characterised in the solid state.

The combined analysis of the X-ray and ESR data for the d^9 species $[Rh(dppf)_2]$, and its iridium analogue, shows a linear dependence of the metal–phosphorus bond distances and the coupling constants of the unpaired electron with the phosphorus nuclei. This observation suggests the possibility to correlate the phosphorus coupling with the metal–phosphorus bond length in similar complexes.

4. Supplementary material

Crystallographic data for structural analysis have been deposited with the Cambridge Crystallographic Data Centre, CCDC nos. 159537 and 159538 for compounds **2** and **3**, respectively. Copies of this information may be obtained free of charge from The Director, CCDC, 12 Union Road, Cambridge, CB2 1EZ, UK (Fax: +44-1223-336033; e-mail: deposit@ccdc.cam.ac.uk or www: http://www.ccdc.cam.ac.uk).

Acknowledgements

The Ministero dell'Universita' e della Ricerca Scientifica e Tecnologica (Pharmacological and Diagnostic Properties of Metal Complexes) is gratefully acknowledged.

References

[1] (a) F.H. Jardine, in: G. Wilkinson, R.D. Gillard, J.A. McCleverty (Eds.), Comprehensive Coordination Chemistry, vol. 4, Pergamon Press, Oxford, 1987, p. 901;
(b) P.R. Sharp, in: E.W. Abel, F.G.A. Stone, G. Wilkinson (Eds.), Comprehensive Organometallic Chemistry II, vol. 8, Pergamon Press, Oxford, 1995, p. 115.

[2] (a) P. Chini, S. Martinengo, Inorg. Chim. Acta 3 (1969) 21;
(b) J.H.B. Chenier, M. Histed, J.A. Howard, H.A. Jolly, H. Morris, B. Mile, Inorg. Chem. 28 (1989) 4114.

[3] (a) J.F. Nixon, B. Wilkins, D.A. Clement, J. Chem. Soc. Dalton Trans. (1974) 1993;
(b) M.A. Bennett, R.N. Johnson, T.W. Turney, Inorg. Chem. 15 (1976) 2938.

[4] H. Caldararu, M.K. DeArmond, K.W. Hank, V.E. Sahini, J. Am. Chem. Soc. 98 (1976) 4455.

[5] (a) E. Makrtik, J. Hanzlik, A. Camus, J. Org. Chem. 142 (1977) 95;
(b) J. Orsini, W.E. Geiger, J. Electroanal. Chem. 380 (1995) 83.

[6] (a) G. Pilloni, G. Zotti, S. Zecchin, J. Organomet. Chem. 317 (1986) 357;
(b) G. Pilloni, E. Vecchi, M. Martelli, J. Electroanal. Chem. 45 (1973) 483;
(c) G. Pilloni, G. Zotti, M. Martelli, Inorg. Chem. 21 (1982) 1283.

[7] (a) A.J. Kunin, E.J. Nanni, R. Eisenberg, Inorg. Chem. 24 (1985) 1852;
(b) G.C. Johnston, M.C. Baird, J. Organomet. Chem. 314 (1986) C51;
(c) B. Bogdanovic, W. Leitner, C. Six, U. Wilczok, K. Wittmann, Angew. Chem. Int. Ed. Engl. 36 (1997) 502.

[8] (a) G.N. George, S.I. Klein, J.F. Nixon, Chem. Phys. Lett. 108 (1984) 627;
(b) K.T. Mueller, A.J. Kunin, S. Greiner, T. Henderson, R.W. Kreilick, R. Eisenberg, J. Am. Chem. Soc. 109 (1987) 6313.

[9] (a) H. Schönberg, S. Boulmaâz, M. Wörle, L. Liesum, A. Schweiger, H. Grützmacher, Angew. Chem. Int. Ed. 37 (1998) 1423;
(b) S. Deblon, S. Boulmaâz, M. Mlakar, H. Schönberg, H. Grützmacher, XXXIII International Conference on Coordination Chemistry, abstract 245, Florence, Italy, 1998.

[10] B. Longato, L. Riello, G. Bandoli, G. Pilloni, Inorg. Chem. 38 (1999) 2818.

[11] (a) U. Casellato, B. Corain, R. Graziani, B. Longato, G. Pilloni, Inorg. Chem. 29 (1990) 1193;
(b) V. Di Noto, G. Valle, B. Zarli, B. Longato, G. Pilloni, B. Corain, Inorg. Chim. Acta 233 (1995) 165.

[12] J.L. Herde, J.C. Lambert, C.V. Senoff, Inorg. Synth. 15 (1974) 18.

[13] G.M. Sheldrick, SHELXTL/PC version 5.03, Siemens Analytical X-ray Instruments Inc., USA, Madison, WI, 1994, Program for Crystal Structure Determination; University of Cambridge, 1980.

[14] G.M. Sheldrick, SHELXTL 93, Program for the Refinement of Crystal Structures, University of Göttingen, Göttingen, Germany, 1993.

[15] J.A. De Gray, P.H. Rieger, N.G. Connelly, G. Garcia Herbosa, J. Magn. Reson. 88 (1990) 376.

[16] M.P. Castellani, N.G. Connelly, R.D. Pike, A.L. Rieger, P.H. Rieger, Organometallics 16 (1997) 4369.

[17] M. Geoffrey, E.A.C. Lucken, Mol. Phys. 22 (1971) 257.